Lekakou, C., Smith, P., Sordon, A., Santoni, C., Meeks, G., & Hamerton, I. (2018). Methods for Process-related Resin Selection and Optimisation in High-Pressure Resin Transfer Moulding. *Materials Science and Technology*. https://doi.org/10.1080/02670836.2018.1557916

Methods for Process-related Resin Selection and Optimisation in High-Pressure Resin Transfer Moulding

Mathew Rutt[a,b]*, C. Lekakou[a], P.A. Smith[a], A. Sordon[b], C. Santoni[b], G. Meeks[b] and I. Hamerton[c]

[a]*Department of Mechanical Engineering Sciences, University of Surrey, Guildford, UK;*
[b]*McLaren Technology Centre, Woking, UK;*
[c]*Bristol Composites Institute (ACCIS), Department of Aerospace Engineering, School of Civil, Aerospace, and Mechanical Engineering, University of Bristol, UK*

*email of the corresponding author: m.rutt@surrey.ac.uk

Short biographical notes on all contributors:

Mathew Rutt graduated with a Master of Chemistry, MChem, at the University of Surrey in 2014. He has been studying for an EngD at the University of Surrey and is an EngD engineer at the McLaren Technology Centre. His research focusses on process development and optimisation of materials and processing conditions in production-scale RTM.

Constantina Lekakou is a Reader at the University of Surrey. She completed her PhD in the Department of Chemical Engineering at Imperial College. London. Her expertise covers the areas of multi-materials processing and manufacturing of polymer composites, and modelling of the transport of species in multiple disciplines including permeation through and across textiles.

Paul Smith is Professor of Composite Materials at the University of Surrey and the Executive Dean of the Faculty of Engineering and Physical Sciences. He holds a first Degree in Engineering and a PhD from the University of Cambridge. His research interests focus on the mechanical behaviour of composite materials.

Alessandro Sordon is a Principal Structural Engineer within the Body in White department at McLaren Automotive. He is responsible for the structural performance of composite and metallic structures, with particular focus on the testing and simulation of composite materials.

Claudio Santoni is Technical Director at the McLaren Automotive Composites Technology Centre. Over the last two decades, he has mainly focussed his work on lightweight automotive body design, materials, processing technology and mass production systems development and implementation.

Graham Meeks is the head of Body Engineering at McLaren Automotive. With over 20 years of experience in the industry, he is responsible for body structures and panels as well as the interior and body systems used in McLaren Automotive's vehicles.

Ian Hamerton is Professor of Polymers and Composite Materials at the University of Bristol and the Research Coordinator/Deputy Director of the ACCIS CDT. He holds a BSc in Chemistry and a PhD from the University of Surrey. His research is concerned with developing polymeric materials with improved performance suitable for use in demanding environments and technologically relevant applications.

Methods for Process-related Resin Selection and Optimisation in High-Pressure Resin Transfer Moulding

A framework for process-related resin selection and optimisation is proposed in the context of research and development for industrial applications of high-pressure resin transfer moulding (HP-RTM). The first stage involves the validation of the reaction kinetics model by differential scanning calorimetry (DSC) and the characterisation of viscosity, storage- and viscous shear-moduli by dynamic mechanical analysis (DMA) in a rheometer as a function of time. Capillary pressure measurements were obtained using a curing resin impregnating a vertical fibre yarn. Process-related resin selection criteria are based on the optimisation of cycle time, including filling time against gel time, micro-infiltration time and demould time. The proposed framework and the associated test and analysis methodologies have been applied to three epoxy resin systems in connection with carbon fibre reinforcement.

Keywords: RTM; composites processing; epoxies; curing; reaction kinetics; DMA; rheology; capillary pressure; optimisation

Subject classification codes: 7: Composite materials

1. Introduction

The application of resin transfer moulding (RTM) in an industrial scale production line requires the constituent materials to be used to their greatest effect in an optimised process [1]. Different reinforcements and resins may be used in RTM and for each type of material there are many varieties and grades available commercially [1–4]. Subsequently, resin screening necessitates lengthy programmes of experimentation or complex computer simulations [5–9]. However, it is possible to develop a methodology involving a faster and more simplified analysis in circumstances where the resin screening exercise is undertaken in conjunction with a mould design and reinforcement that are well known and have been previously optimised. The aim of this study has been to assemble a framework for process-related resin selection and optimisation for a given

RTM mould and fibre reinforcement. In this framework, set requirements may be modified regarding mechanical and other properties of the RTM composite product, filling length and filling time, total cycle time, demould time and post-cure time.

The proposed methodology is demonstrated in this study for different types of epoxy systems, which constitute a class of polymers that are used in industry not only as composite matrices, but also in paints, coatings and adhesives [10–12]. Their extensive use can be attributed to their numerous desirable properties: high modulus, high strength and (depending on structure) high glass transition temperature (*Tg*) [13–16]. In order to enhance the quality and productivity of RTM, the interdependency of all aspects contributing to the process as a whole must be understood [1, 6, 17–19]. The first area to be considered must be the current processing parameters and the desired enhancement. Simply taking the size of the target component, for example, small components can be easily formed using RTM with 'snap cure' resin systems. Such systems often employ highly reactive epoxy resins or polyurethane systems [20–23], which require dynamic curing parameters due to their highly reactive nature, the lower temperature allowing for the infusion of the resin followed by an increase in temperature to cure. Alternatively, for large complex components which lend themselves well to RTM processing, the user will be limited to isothermal processing as it is not generally economical to vary the temperature of a large RTM mould, despite the recent development of induction heating for mould surfaces [24]. The consequence is that the resin screening framework for the RTM of large automotive components can be based on isothermal resin curing.

Issues observed during the infusion stage in an isothermal process include achieving full resin infusion prior to the resin reaching its gel point whilst ensuring processing times are maintained as short as possible [21, 25–27]. In order to achieve

the high rates of resin injection required, state-of-the-art equipment must be used such as injection systems primarily used for polyurethane processing. Current, commercially-available high-pressure resin transfer moulding (HP-RTM) systems boast injection heads capable of 12 kg/min with a low-pressure radial piston pump feeding a high-pressure pump capable of rates of 36 kg/min, and the equipment withstanding pressures exceeding 200 bar [28].

The resin flow during the stage of impregnation of the fibre reinforcement by the resin is governed by Darcy's law [29]:

$$\boldsymbol{U} = \frac{[\boldsymbol{K}]}{\mu\varepsilon}\nabla P \tag{1}$$

where $\boldsymbol{U}$ is the velocity vector indicating the progress of the flow front, $[\boldsymbol{K}]$ is the permeability tensor of the fibre reinforcement, ε is the average porosity of the fibre reinforcement, μ is the resin viscosity (Newtonian fluid), and ∇P is the pressure gradient in all directions. In resin screening, for a set geometry and fibre reinforcement, the velocity and, subsequently, the impregnation time would depend on the resin viscosity which would, in turn, be affected by the degree of curing. Ultimately, the degree of curing, governed by the reaction kinetics, would control both the gel time and the time at which the polymer composite would reach the required *Tg* and mechanical properties.

An additional issue, prominent in HP-RTM, is a distinct difference between the flow fronts of the macro-flow (between fibre tows or fibre bundles) and micro-flow (between fibres within a fibre tow or a fibre bundle) [6, 30-31], which depends primarily on the ratio of macro- and micro-permeabilities of the fibre reinforcement. The total impregnation time then includes the completion of the micro-impregnation within the fibre tows or yarns in and near the last filled region of the fibre

reinforcement, *i.e.* by the flow front. Micro-infiltration of the fibre tows or yarns takes place mainly transversely to the fibres [30] and is induced by the capillary pressure at the flow front and vacuum pressure, if it is applied, whereas the effect of injection pressure is less significant at the micro-flow front [30].

Hence, a framework is presented in this study for the process-related resin selection for a given mould and fibre reinforcement, based on the ability of the resin to fully fill the mould and fully impregnate the reinforcement without any premature gelling, voids or micro-voids, to minimise the overall cycle time in the mould (filling and curing) while guaranteeing demoulding a composite product with optimum structural and mechanical performance.

2. Materials and Methods

Three epoxy-based matrix systems were investigated in the development of the resin screening method. Resin (a) supplied by Huntsman was XB6469 resin using cure agent Aradur 2954. Resin (b) again from Huntsman was Araldite LY1564 resin using curing agent Aradur 22962. Finally, resin (c) supplied by Gurit was T-Prime 130-1 resin using T-Prime 130-1 hardener.

Differential scanning calorimetry (DSC) experiments were carried out to determine the type of reaction kinetics (catalytic described by equation (2) or autocatalytic described by equation (3)) [32] and the reaction constants for each resin system.

$$Catalytic\ reaction: \quad \frac{d\alpha}{dt} = k(1-\alpha)^n \tag{2}$$

$$Autocatalytic\ reaction: \quad \frac{d\alpha}{dt} = k\alpha^m(1-\alpha)^n \tag{3}$$

where α is the extent of cure as a function of time, *t*, *m* and *n* are constants indicating

the order of reaction processes, and k is the rate constant following Arrhenius temperature dependence according to relation (4), where A is the frequency factor, Ea is the reaction activation energy, T is the absolute temperature and R is the gas constant.

$$k = Ae^{-Ea/RT} \tag{4}$$

TA instruments Q1000' DSC equipment was used and measurements were made at the imposed temperature ramp rates, β, of 5,7.5,10,12.5 and 15 K min^{-1} from ambient temperature to 280 ^{o}C. The activation energy, Ea, and the pre-exponential factor, A, were determined using equation (4) according to two different methods, the Ozawa method [33] and the Kissinger method [34]. Further analysis of the experimental data of the dynamic DSC was conducted to determine the type and order of reaction in equation (2) or (3). Isothermal DSC was conducted at 85 ^{o}C (the temperature of isothermal RTM in this study) for the validation of the reaction kinetics model and reaction constants previously determined.

Dynamic mechanical analysis (DMA) tests of the resin systems were carried out using a TA instruments DHR-1 Rheometer and 25 mm parallel plate geometry in a frequency sweep at a strain of 10% and different times to provide data for the storage and viscous shear modulus, G' and G'', respectively, as a function of curing time.

DMA tests at the low frequencies, f = 0.1 Hz and 1 Hz, were conducted to characterise the rheology of each curing resin and determine the viscosity, μ, as: $\mu = G''/\omega$ where ω is the angular frequency (in rad s^{-1}). From graphs of viscosity against time, then, the maximum filling time can be determined before μ reaches a critical value, beyond which, the viscosity is not allowed to rise. Above this critical viscosity value, processing problems may then be observed for a given mould and reinforcement combination; such as slow filling and incomplete impregnation before gelling. Given

than the viscosity is a function of temperature and degree of curing: $\mu = \mu_{oT}\mu_{oX}$, the data were used to fit and determine the constants of the following equations describing the curing system rheology [32, 35-36]:

$$\mu = \mu_{oT}\left(\frac{\alpha_g}{\alpha_g - \alpha}\right)^{B+C\alpha} \quad (5)$$

$$\mu = \mu_{oT}e^{B\alpha} \quad (6)$$

where α_g is the degree of curing at the gel point and μ_{oT} depends on temperature according to:

$$\mu_{oT} = \mu_o e^{Ev/RT} \quad (7)$$

DMA tests at the high frequency of 100 Hz were used to determine the storage shear modulus, *G'*, as a function of curing time for each resin system. From graphs of *G'* against time, the demould time can be determined using a minimum value of G'. This is related to the minimum state of curing at which a given composite product can be demoulded; without damage or distortion.

Measurements of the capillary pressure of each resin, P_{cII}, parallel to the fibres were carried out by measuring the mass of each curing epoxy system rising into a carbon fibre bundle, following the methodology and using the equipment described by Amico and Lekakou [37]. However, as this is the first time in the literature that the P_c of a curing system has been determined, the change of viscosity as a function of curing following equation (5) or (6) has been taken into account in equation (8a) or (8b), respectively:

$$\left(\frac{\alpha_g}{\alpha_g - \alpha}\right)^{B+C\alpha}\frac{dW}{dt} = \frac{K\rho^2 A_{TV}^2 P_{cII}}{\mu_{oT}\varepsilon}\frac{1}{W} - \frac{K\rho^2 A_{TV} g}{\mu_{oT}\varepsilon} \quad (8a)$$

$$e^{B\alpha}\frac{dW}{dt} = \frac{K\rho^2 A_{TV}^2 P_{cII}}{\mu_{oT}\varepsilon}\frac{1}{W} - \frac{K\rho^2 A_{TV} g}{\mu_{oT}\varepsilon} \quad (8b)$$

where W is the mass of the bundle being impregnated with resin against time t, ρ is the resin density, A_{TV} is the pore area of the bundle cross-section (determined from image analysis of cross-sections of the cured epoxy-impregnated carbon fibre bundle) and g is the [acceleration due to] gravity. After taking the measurements and calculating α against time from the reaction kinetics of each epoxy system, the left-hand side of equation (8a) or (8b) was plotted against $1/W$ and a straight line was fitted through the data of which the gradient a_w and intercept b_w were determined. The capillary pressure was then determined from equation (9):

$$P_{cII} = \frac{a_w}{b_w}\frac{g}{A_{TV}} \quad (9)$$

Given that for a short time initially in the capillary experiments the viscosity may be constant and the gravity term may be ignored, equations (8) may be integrated into the following simplified equation, the gradient of which would be $2\alpha_w \mu_{oX}$:

$$W^2 = \frac{2K\rho^2 A_{TV}^2 P_{cII}}{\mu_{oT}\mu_{oX}\varepsilon} t \quad (10)$$

3. Results

3.1 Reaction kinetics

Figure 1 displays an example of data analysis to determine the reaction kinetics for resin system (a). The results of dynamic DSC (Figure 1(a)) were fitted according to the Ozawa [33] and Kissinger method [34] (Figure 1(b)) to determine the reaction activation energy as: Ea = 63.4 kJ/mol and Ea = 60.0 kJ/mol, respectively, as well as

the pre-exponential factor $A = 22.5 \times 10^6$ min^{-1}. A catalytic reaction of equation-type (2) fitted the data of Figure 1(a) only after the peak exotherm, whereas an autocatalytic reaction of equation-type (3) fitted a larger portion of the data (Figure 1(c)) with optimised values of constants: $m = 0.15$ and $n = 0.8$. The so determined reaction kinetics parameters were inputted in equations (3) and (4) to predict the extent of reaction versus time for the isothermal DSC at 85 ^{o}C and these predictions compare very well with the corresponding experimental data for system (a) as is shown in Figure 1(d). Table 1 presents the reaction kinetics model constants and parameters for all three investigated epoxy resin systems, determined as illustrated in Figure 1. All three epoxy systems appear to follow autocatalytic reaction kinetics.

3.2 Results of the dynamic mechanical analysis (DMA) tests

Figure 2 presents an example of viscosity data for resin system (a) at 85 ^{o}C and at two different frequencies, 0.1 and 1 Hz: the 0.1 Hz frequency appears to capture the viscosity rise at gel point early and is in fact closer to the state of slow flow conditions present at RTM, hence, it was used for the viscosity measurements of all resin systems at 85 ^{o}C which are presented in Figure 3. The rheology models of viscosity against the degree of curing, described by the alternative equations (5) and (6), were fitted to the experimental data for each resin system with the derived model parameters displayed in Table 2. The corresponding viscosity predictions against time are shown in Figure 3 (as well as the predicted progress of curing) where it can be seen that both equations (5) and (6) fit well the experimental data for resin system (b), equation (6) fits better for resin system (a) and equation (5) fits better for resin system (c).

Figure 4 presents the experimental data of the shear storage modulus, G', versus time during DMA tests at 100 Hz for the three epoxy resin systems curing isothermally at 85 ^{o}C. Epoxy systems (a) and (b) exhibit a fast rise of G' after the gel point, followed

by some reduction after 4 MPa which we suspect is due to the detachment of the solid specimen from the rotating disk plates of the DMA instrument. System (c) demonstrates a steady rise of G' with available data values above 10 MPa.

3.3 Results of the capillary pressure tests

Figure 5 presents the experimental data for all resin-curing agent systems. The data at the start of the impregnation (when the effect of gravity may be neglected) were fitted linearly in plots of W^2 versus time, t, following equation (10), when the gradient represents $2\alpha_w \mu_{oX}$ from which α_w was determined. The data were then converted into the x- and y- axes of equation 8 and best fit lines were drawn with gradient α_w as previously determined; their intercept (if negative) represented b_w. In two experiments with resin system (b), the equilibrium weight, We, was reached (dW/dt =0), in which case the intercept was determined as: $b_w = \alpha_w/W_e$. The best fit equations were also employed in the calculation of predicted weight against time via numerical integration of equation (8): the predictions are presented against the experimental data in the bottom row of graphs in Figure 5. Differences between repeat experiments and also between the best fits and the experimental data can be detected. After some initial time it is suspected that the resin impregnation may enlarge the fibre yarn cross-section and subsequently increase the porosity that would reduce the capillary pressure and, hence, the rate of resin rise (resins (b) and (c)) or would increase the permeability and facilitate the flow of a low viscosity resin (resin (a)). Table 3 presents the determined values of the capillary pressure, P_{cII}, parallel to the fibres for each resin/curing agent system, determined after inputting an average value for porosity (ε = 0.725) and A_{TV}, derived from image analysis of cured impregnated carbon fibre yarn cross-sections as in Figure 6(a): it appears that resin systems (b) and (c) have the lowest and highest P_{cII} values, respectively.

4. Discussion

The proposed framework for process-related resin selection in isothermal HP-RTM for a given mould and fibre reinforcement is based on a first stage of experimental studies to establish reaction kinetics, viscosity and shear storage modulus as a function of curing time and capillary pressure at known porosity value as outlined in Section 2 and demonstrated in Section 3. The next stage includes the process of resin screening to minimise filling and demould time and ensure full macro- and micro-infiltration of the fibre reinforcement at the end of filling.

Demould time is a key part of the cycle time and cost as it represents the utilisation time of each RTM mould, which defines the production rate. Considering the rise of shear storage modulus at the process temperature in Figure 7(a), it can be determined when the composite is sufficiently cured for demoulding. If the demould time of the RTM polymer composite product had been optimised for resin (a), for example, to 65 min, this corresponds to G'=3.47 MPa. This value for G' is reached at 28 min for resin (b) and at 128 min for resin (c). Resin (b) seems to compare favourably against the other two resins in terms of achieving time- and cost-effective RTM production.

With regards to gel time against infiltration time, the three systems all display a low starting viscosity but differ in terms of the start of gel time as is shown in Figure 3. Depending on the maximum filling time requirement, one may choose all or narrow the selection to complete filling during RTM before resin gel occurs. As shown in Figure 7(b), if for example, the RTM process had been optimised initially for resin (a) to a filling time of 20 min corresponding to a viscosity of about 1 Pa s at the end of filling, resins (b) and (c) reach that viscosity after about 10 min, which means that the filling time would need to be reduced to 10 min to avoid gelling or too slow impregnation; this might be achieved by increasing the injection pressure, for example.

Micro-infiltration should also be completed before gelling, fibre yarns near the macroscopic flow front at the end-of-fill are the last to be impregnated via micro-infiltration. In the case of multiple layers of unidirectional fibres or in stitch-bonded fabrics, layers and yarns are highly compressed, at ε = 0.05-0.4, and micro-infiltration times may be 20% of the filling time in HP-RTM [30]. Application of vacuum aids not only micro-infiltration but also accelerates macro-infiltration, which ultimately increases the difference between the flow fronts of macro- and micro-infiltration and causes additional delays of micro-infiltration after the filling in the form of macro-infiltration is complete. Capillary pressure is beneficial as it induces only micro-flow and is negligible in the macro-channels. According to the Young-Laplace equation [37], the capillary pressure is proportional to: $F(1-\varepsilon)/\varepsilon$ where F = 4 or 2 for flow parallel or perpendicular to the fibres, respectively. On that basis and following from the experimental data of P_{cII}, the values of both P_{cII} and P_{cT} have been calculated for different possible values of micro-porosity, ε, of carbon fibre yarns and are displayed in Table 3. Micro-flow is accomplished mainly under capillary pressure transverse to the fibres, Pc_T. As seen in Table 3, at a micro-porosity ε = 0.1, resins (c), (a) and (b) exert a transverse capillary pressure of 0.4 bar, 0.2 bar and 0.02 bar, respectively, which means that the corresponding micro-infiltration times are related as: 1:2:20. Hence, while resin (b) may offer distinct advantages in terms of quick gelling and early demould time, care must be taken to complete micro-infiltration and ensure the absence of microvoids.

5. Summary

Using the proposed frame work, three epoxy resin systems were assessed for their relative suitability in an HP-RTM process with respect to processing; in the infiltration, curing and demoulding stages. Their reaction type (catalytic/autocatalytic) was

established and in the case of resin system (a), a high level of agreement was seen between theoretical calculations of reaction extent when compared with experimental data. Viscosity and shear storage modulus data used with capillary pressure studies supplied valuable data used in the optimisation of the mould-filling stage of HP-RTM. Further storage modulus data provided insight into the possibility of cycle time optimisation with respect to minimum G' values for demould.

Through the creation and validation of the framework in this study; the screening process and optimisation of resin systems for HP-RTM can be carried out consistently and with increased efficiency. The epoxy resin of choice can be utilised to greater effect allowing the overall cost of optimisation and target process to be carried out more efficiently.

Acknowledgements

This work is part of the EngD Programme in Micro- and NanoMaterials and Technologies at the University of Surrey. The authors gratefully acknowledge the financial support by EPSRC under Grant Agreement EP/L016788/1.

References

1. Swentek I, Beck B, Ugresic V, et al. Impact of HP-RTM process parameters on mechanical properties with epoxy and polyurethane systems. Sampe J. 2017;53: 20-25.
2. Kobayashi S, Tsukada T, Morimoto T. Resin impregnation behavior in carbon fiber reinforced polyamide 6 composite: Effects of yarn thickness, fabric lamination and sizing agent. Compos. Part A Appl. Sci. Manuf. 2017;101: 283–289.
3. Potter K. Resin Transfer Moulding, London, Chapman & Hall, 1997.
4. Hesabi M, Salimi A, Beheshty MH. Effect of tertiary amine accelerators with different substituents on curing kinetics and reactivity of epoxy/dicyandiamide system. Polym. Test. 2017;59: 344–354.

5. Yeager M, Hwang WR, Advani SG. Prediction of capillary pressure for resin flow between fibers. Compos. Sci. Technol. 2016;126: 130–138.
6. Imbert M, Abisset-Chavanne E, Comas-Cardona S, et al. Efficient dual-scale flow and thermo-chemo-rheological coupling simulation during on-line mixing resin transfer molding process. J. Compos. Mater. 2018;52: 313–330.
7. Pierce RS, Falzon BG. Simulating resin infusion through textile reinforcement materials for the manufacture of complex composite structures. Engineering. 2017;3: 596–607.
8. Bruschke MV, Advani SG. A finite-element control volume approach to mold filling in anisotropic porous-media. Polym. Compos. 1990;11: 398–405.
9. Lekakou CN, Richardson SM. Simulation of reacting flow during filling in reaction injection moulding (RIM). Polym. Eng. Sci. 1986;26: 1264-1275.
10. Duan Y, Huo Y, Duan L. reparation of acrylic resins modified with epoxy resins and their behaviors as binders of waterborne printing ink on plastic film. Colloids Surfaces A-Physicochemical Eng. Asp. 2017;535: 225-231.
11. Giaveri S, Gronchi P, Barzoni A. IPN Polysiloxane-epoxy resin for high temperature coatings: structure effects on layer performance after 450 degrees C treatment. Coatings. 2017;7: 1-16.
12. Trimino LF, Cronin DS. Damage measurements in epoxy structural adhesives using microhardness. Int. J. Adhes. Adhes. 2018;82: 211-220.
13. Friedrich K, Almajid AA. Manufacturing aspects of advanced polymer composites for automotive applications. Appl. Compos. Mater. 2013;20: 107-128.
14. Shi H-Q, Sun B-G, Liu Q, et al. A high ductility RTM epoxy resin with relatively high modulus and Tg. J. Polym. Res. 2015; 22: 134 1-9.
15. Downey MA, Drzal LT. Toughening of aromatic epoxy via aliphatic epoxy copolymers. Polymer. 2014;55: 6658-6663.
16. Wang M, Xu X, Ji J, et al. The hygrothermal aging process and mechanism of the novolac epoxy resin. Compos. Part B-Engineering. 2016;107: 1-8.

17. Zhang C, Kang N, Li L, et al. Case study of SUV hatchback: `material-structure-process performance' integration design and numerical verification of automotive composite components. Proceedings of the 2017 ASME International Mechanical Engineering Congress and Exposition, 2017 Nov 3-9; Tampa, Florida. ASME; 2018; vol.11.
18. Yalcinkaya MA, Sozer EM, Altan MC. Fabrication of high quality composite laminates by pressurized and heated-VARTM. Compos. Part A-Applied Sci. Manuf. 2017;102: 336-346.
19. Schillfahrt C, Fauster E, Schledjewski R. Influence of process pressures on filling behavior of tubular fabrics in bladder-assisted resin transfer molding. Adv. Manuf. Compos. Sci. 2017: 148-158.
20. Wang Y, Lakho DA, Yao D. Effect of additives on the rheological properties of fast curing epoxy resins. Ep. J. Silic. Based and Compos. Mater. 2015;67: 132-134.
21. Deléglise M, Le Grognec P, Binetruy C, et al. Modeling of high speed RTM injection with highly reactive resin with on-line mixing. Compos. Part A Appl. Sci. Manuf. 2011;42: 1390-1397.
22. Hong B, Xian G. Ageing of a thermosetting polyurethane and its pultruded carbon fiber plates subjected to seawater immersion. Constr. Build. Mater. 2018;165: 514-522.
23. Park S-K, Kim C-H, Choi J-H. A study on cure monitoring of fast cure resin RTM process using dielectrometry. Compos. Res. 2017;30: 202-208.
24. Feigenblum J, Senmartin J. RTM technology improvement with tool surface heating by induction. FPCM-9-The 9th International Conference on Flow Processes in Composite Materials; 2008 Jul 8-10; Montréal (Québec), Canada.

25. Okabe T, Oya Y, Yamamoto G, et al. Multi-objective optimization for resin transfer molding process. Compos. Part A-Applied Sci. Manuf. 2017; 92: 1-9.
26. Di Fratta C, Koutsoukis G, Klunker F, et al. Fast method to monitor the flow front and control injection parameters in resin transfer molding using pressure sensors. J. Compos. Mater. 2016;50: 2941-2957.
27. Han SH, Cho EJ, Lee HC, et al. Study on high-speed RTM to reduce the impregnation time of carbon/epoxy composites. Compos. Struct. 2015;119: 50-58.
28. Krauss Maffei, "No Title." [Online]. Available from: http://www.kraussmaffei.de/en. [Accessed: 08-Sep-2016].
29. Darcy HPG. Les fontaines publiques de la Ville de Dijon. Paris, France: Dalmont; 1856.
30. Lekakou C, Bader MG. Mathematical modelling of macro- and micro-infiltration in resin transfer moulding (RTM). Composites Part A-Applied Sci. Manuf. 1998;29A: 29-37.
31. Amico S, Lekakou C. Flow through a two-scale porosity, oriented fibre porous medium. Transport in Porous Media. 2004;54: 35-53.
32. Lekakou CN, Richardson SM. Simulation of the filling and curing stages in RIM: sensitivity analysis on reaction kinetics, Plast. Rubb. Proc. Appls. 1988;10: 17-25.
33. Ozawa T. A new method of analyzing thermogravimetric data. Bull. Chem. Soc. Japan. 1965;38: 1881-1886.
34. Kissinger HE. Reaction kinetics in differential thermal analysis. Analytical Chemistry. 1957;29: 1702-1706.
35. Castro JM, Macosko CW. Studies of mould filling and curing in the reaction injection moulding process. AIChe J. 1982;28: 250-260.

36. Sibal PW, Camargo RE, Macosko CW. Designing nylon-6 polymerisation systems for RIM. Pol. Proc. Eng, 1983-84;1: 147-169.
37. Amico SC, Lekakou C. Axial impregnation of a fiber bundle. Part 1: Capillary experiments. Polymer Composites. 2002;23: 249-263.

LIST OF TABLES

LIST OF FIGURES

Figure 6. Composite cross-sections: (a) cross-section of cured impregnated free fibre bundle in capillary experiments with determined $\varepsilon = 0.725$ and $A_{TV} = 378490$ µm^2, (b) part of cross-section of epoxy-stitch-bonded carbon fibre composite produced by RTM.

Figure 7. Diagrams demonstrating the relation between process requirements and properties of the curing resin systems

TABLES

Table 1. Curing reaction kinetics model data for the three epoxy systems of this study, determined from the DSC data analysis.

Epoxy system	Reaction equation	A (min^{-1})	Ea (kJ mol^{-1})	K_{85^oC} (min^{-1})	m	n
(a)	(3)	22.5x10^6	60.0	3.94x10^{-2}	0.15	0.80
(b)	(3)	18.8 x10^6	60.2	3.11 x10^{-2}	0.40	1.80
(c)	(3)	7.99 x10^6	58.1	2.65 x10^{-2}	0.40	2.5

Table 2. Chemico-rheological model parameters derived from the rheological tests (at 0.1 Hz and 85 ^{o}C) and the reaction kinetics model of the three epoxy/curing agent systems of this study.

Epoxy system	Model equation	μ_{oT} (Pas)	B	C	α_g
(a)	(6)	0.100	1.0	2.0	0.94
	(7)	0.003	20.3		
(b)	(6)	0.166	35.0	0	0.8
	(7)	0.093	53.7		
(c)	(6)	0.087	42.0	0	0.95
	(7)	0.057	60.8		

Table 3. Experimental data from the determination of the capillary pressure in upwards impregnation of vertical carbon fibre yarn for all resin/curing agent systems at T = 45 ^{o}C, where it was determined experimentally that the cured polymer-carbon fibre composite yarn had ε = 0.725 and A_{TV} = 378490 μm^2. Predicted capillary pressure for different porosity values.

Case	Fibre yarn porosity, ε	Resin (a)		Resin (b)		Resin (c)	
		P_{cII} (Pa)	P_{cT} (Pa)	P_{cII} (Pa)	P_{cT} (Pa)	P_{cII} (Pa)	P_{cT} (Pa)
Experiments	0.725	1614±160		215±70		3530±590	
Predictions	0.30	9928	4964	1322	661	21715	10857
	0.20	17020	8510	2267	1134	37225	18613
	0.15	24112	12056	3212	1606	52736	26368
	0.10	38296	19148	5101	2551	83757	41879

FIGURES

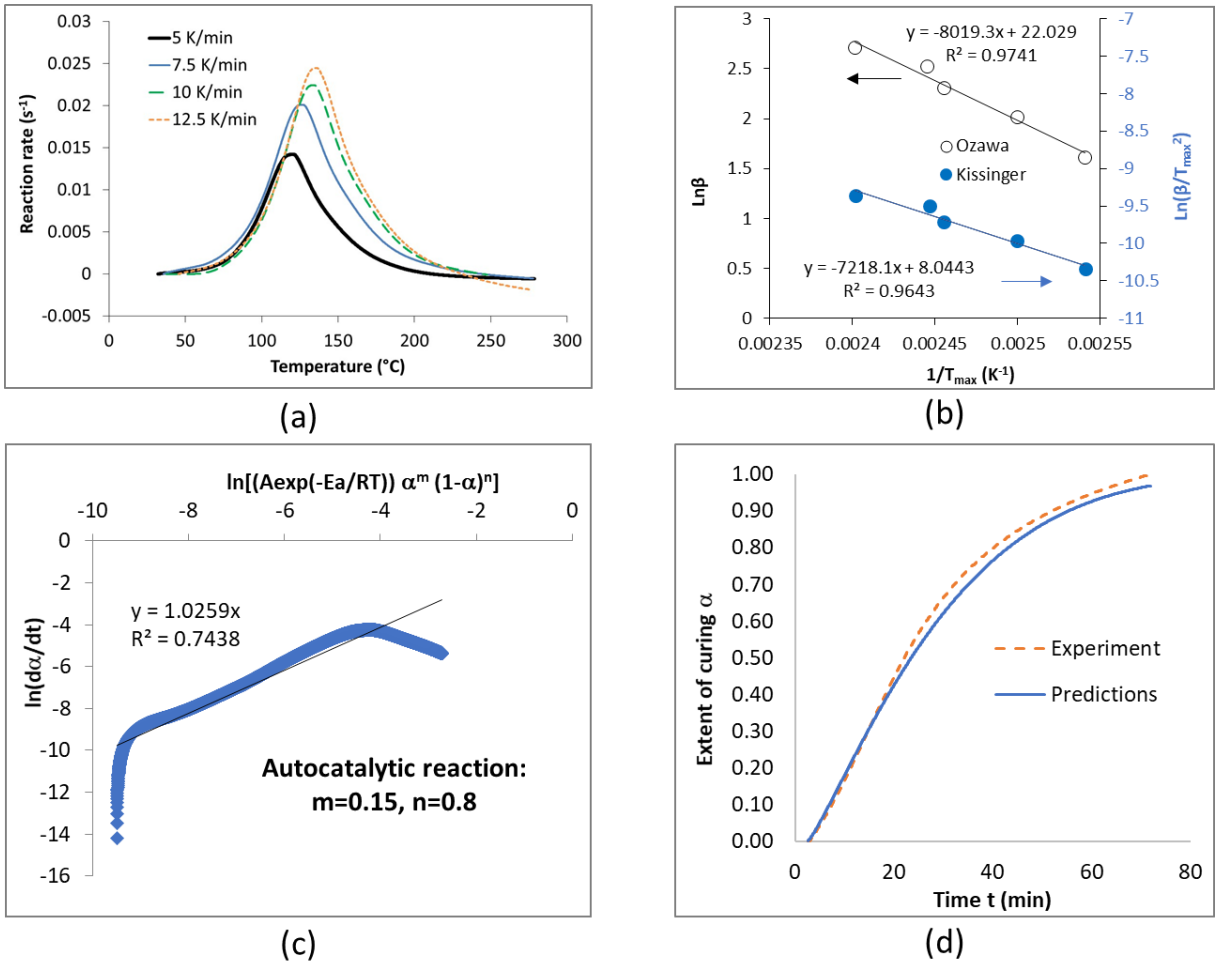

Figure 1. Example of DSC analyses and numerical fitting of experimental data for resin (a): epoxy system XB6469/ Aradur 2954: (a) experimental data of dynamic DSC at different temperature rise rates, β; (b) fitting of the experimental data of dynamic DSC according to the Ozawa method [33] and the Kissinger method [34] to determine *Ea* and *A*; (c) fitting of the dynamic DSC experimental data to obtain the type and order of reaction, in this case autocatalytic type of reaction with determination of *m* and *n* constants; (d) validation of the reaction kinetics model and determined reaction parameters in (b) and (c) by comparing predictions and experimental data in isothermal DSC at 85 ºC.

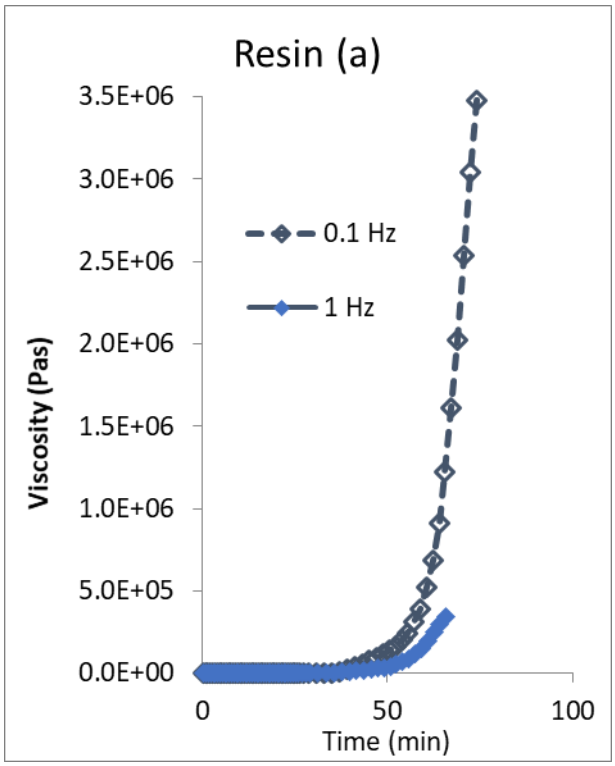

Figure 2. Graphs of experimental viscosity data from DMA tests at 0.1 Hz and 1 Hz and 85 ºC for resin/curing agent system (a).

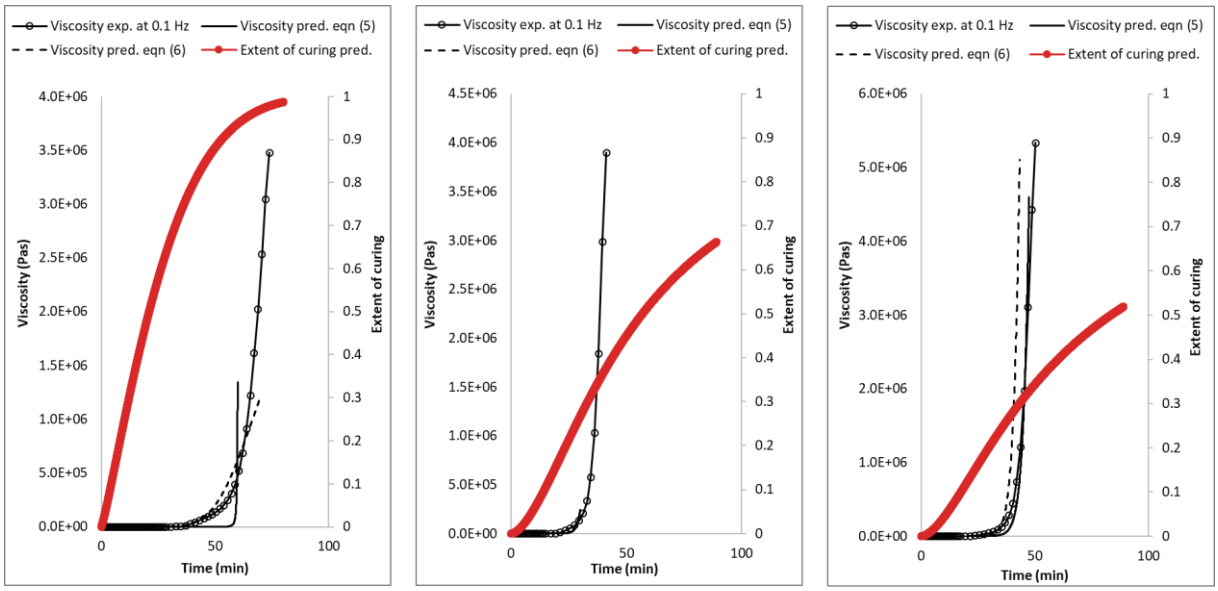

Figure 3. Graphs of viscosity (experimental data from DMA tests at 0.1 Hz and 85 ^{o}C and predictions according to equations (5) and (6)) against time and predicted degree of curing against time according to equation (3) for the three epoxy resin/curing agent systems of this study.

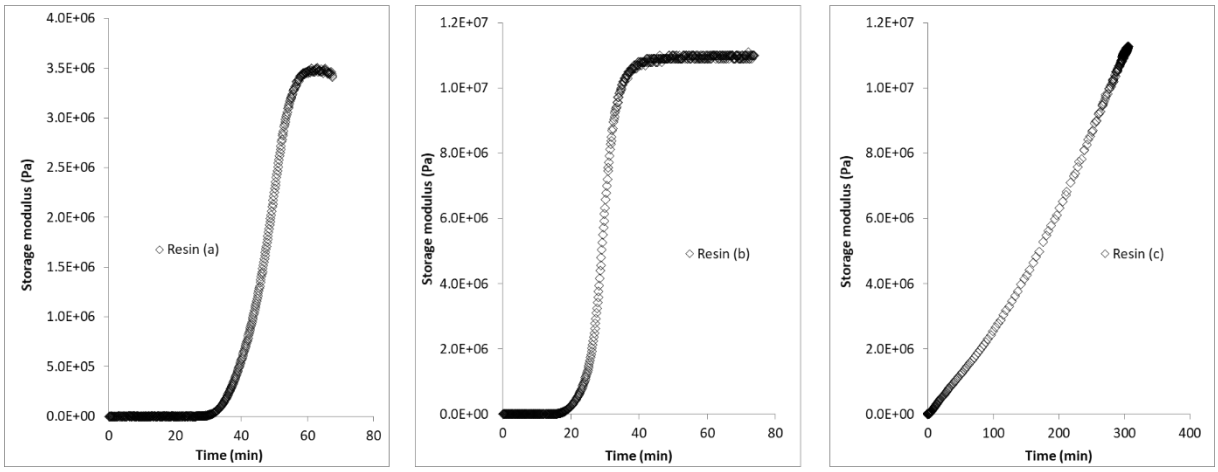

Figure 4. Experimental data of the storage shear modulus as a function of curing time from DMA tests at 100 Hz and 85 ^{o}C for the three epoxy resin/curing agent systems of this study.

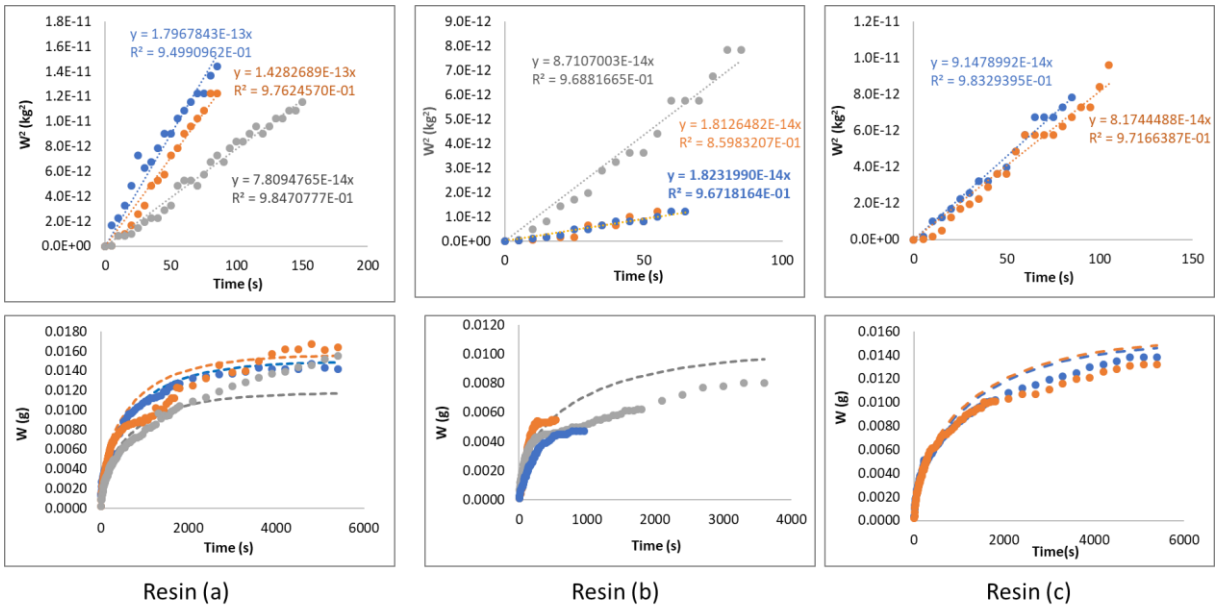

Figure 5. Experimental data and best fits of upwards impregnation experiments of a vertical carbon fibre yarn at T = 45 ºC for all resin/curing agent systems.

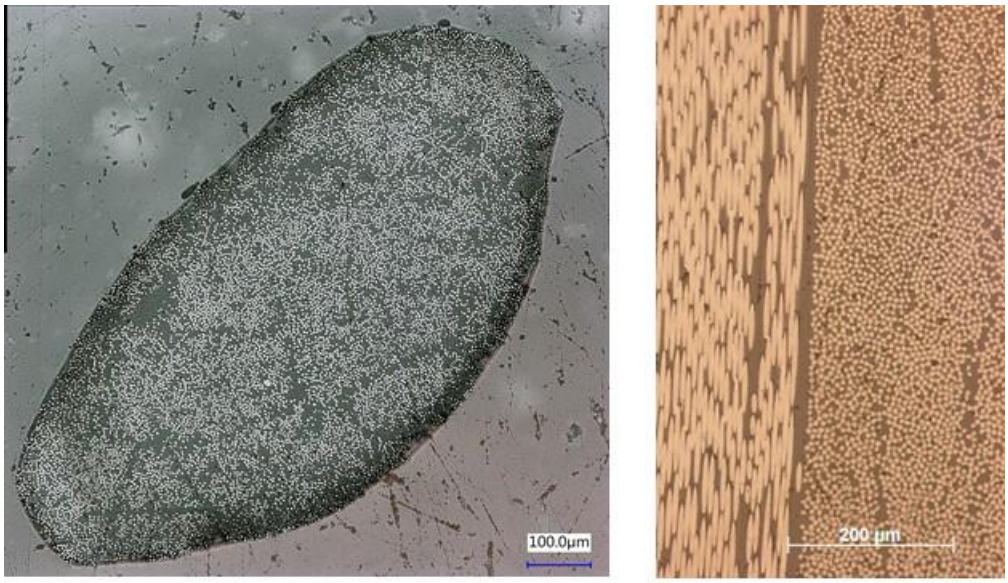

Figure 6. Composite cross-sections: (a) cross-section of cured impregnated free fibre bundle in capillary experiments with determined $\varepsilon = 0.725$ and $A_{TV} = 378490$ µm^2, (b) part of cross-section of epoxy-stitch-bonded carbon fibre composite produced by RTM.

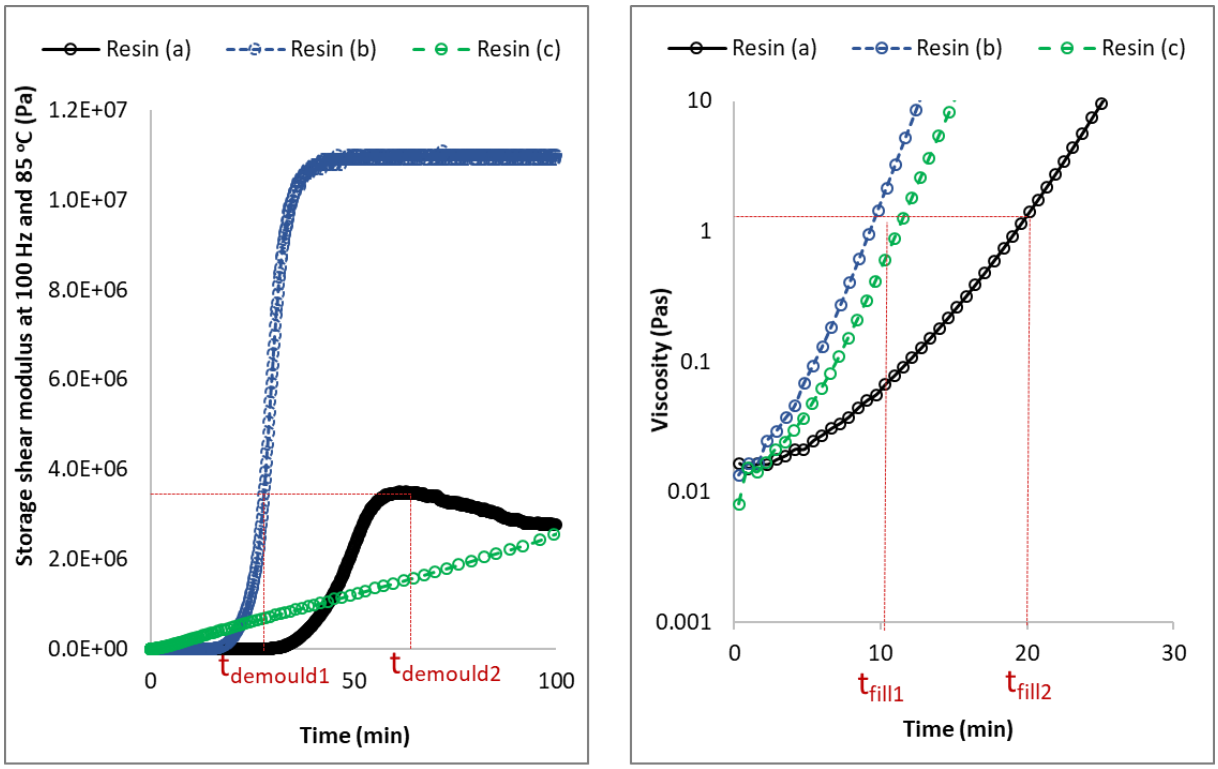

Figure 7. Diagrams demonstrating the relation between process requirements and properties of the curing resin systems